J Mater Sci (2008) 43:2018–2025
DOI 10.1007/s10853-007-2302-6

Anomalous electrical properties of nanocrystalline Ni–Zn ferrite

A. D. Sheikh · V. L. Mathe

Received: 15 July 2007 / Accepted: 6 November 2007

Abstract Nanocrystalline powders of Ni–Zn ferrite (NZFO) having the chemical formula Ni_x Zn_{1-x} Fe_2O_4, where x varies as 1, 0.8, 0.6, 0.4, 0.2, and 0, were synthesized by chemical co-precipitation technique. The samples synthesized were characterized by X-ray diffraction (XRD) technique at several stages. As prepared samples at room temperature show absence of Bragg peak indicating that there was no crystalline phase formation of ferrite. The XRD pattern of the samples sintered at 400 °C clearly showed the characteristic Bragg peaks of spinel cubic structure. XRD patterns were further analyzed to calculate the lattice constant, porosity, and jump length of charge carriers. Electrical dc resistivity measurements were carried out with respect to temperature using two probe method. NZFO samples showed abnormal electrical behavior at room temperature. Also abnormal electrical behavior with increase in temperature in the range 600–800 K was observed. Variation of dielectric constant and loss tangent with frequency were studied at room temperature. The electrical and dielectric behavior of the Ni–Zn samples is discussed in the light of literature.

Introduction

Magnetic nanoparticles continue to be a fascinating subject of interest from both fundamental and application point of view. It is well known that polycrystalline Ni–Zn ferrites (NZFOs) are widely used for many technological applications [1, 2]. Most electronic applications require these materials to be pressed into larger shapes with near theoretical density, which is difficult to obtain if the particles have wide-size distribution [3].

Ni–Zn ferrites are well known and have been used for many years in the electrical and electronic industries. NZFO is a soft magnetic ceramic that has spinel configuration based on a face-centered cubic lattice of the oxygen ions, with the unit cell consisting of eight formula unit of the type $[Zn_xFe_{1-x}]_A$ $[Ni_{1-x}Fe_{1+x}]_B$ O_4. In this formula 'A' represents tetrahedral site and 'B' represents octahedral site [4]. The structural, electrical, dielectric, etc. properties of ferrite are very much sensitive to methodology adopted for the synthesis, preparative parameters, initial ingredients, etc. The change in cation distribution may result into unexpected electrical and magnetic behavior. Nowadays, these materials are largely studied in the search for improved properties [5] and new applications [6] especially in the nanometric scale as ultrafine powders [7] and thin films [8, 9]. Ferrites are commonly produced by a ceramic process involving high-temperature solid-state reactions between the constituent oxides or carbonates. The particles obtained by this process are rather large and non-uniform in size. These non-uniform particles, on compacting, result in the formation of voids or low density. In order to overcome these difficulties arising out of the ceramic route, wet chemical methods like air oxidation, co-precipitation, hydrothermal processing, etc. have been considered for production of homogeneous, fine and reproducible ferrites [10]. In this work, we have studied synthesis of nano-sized ferrimagnetic $Ni_xZn_{1-x}Fe_2O_4$ powder by co-precipitation followed by low- and high-temperature sintering and investigated the structural and electrical properties of the obtained samples. The electric properties of ferrites gives valuable information about the behavior of localized

A. D. Sheikh · V. L. Mathe (✉)
Novel Materials Research Laboratory, Department of Physics, University of Pune, Pune 411 007, Maharashtra, India
e-mail: vlmathe@physics.unipune.ernet.in

electric charge carriers leading to a greater understanding of mechanism of dielectric polarization of the ferrites.

Experimental

The $Ni_xZn_{1-x}Fe_2O_4$ sample was synthesized using Ni nitrate, Zn acetate and Fe nitrate as precursors, by dissolving them in distill water in the required mole proportion. The clear solution was co-precipitated with a 1 molar NaOH solution at fixed temperature of 100 °C. Samples at this stage are refereed 'as prepared'. The precipitate was filtered and then washed several times with distilled water until the pH of the filtered water became 7 (i.e., neutral). The filtrate was then dried at 100 °C overnight. The dried powders were then used to make pellet with a die of diameter 10 mm. The hand press machine was used to apply pressure of about 5–6 ton for 5 min was applied to make the pellets. The diameter of the 2- to 3-mm thick pellet was 10 mm. These pellets were sintered at different sintering temperatures for same interval of time. The data of the pellets structural, electrical, and dielectric properties on the samples sintered at 400 °C was collected. All the samples further sintered at 900 °C for the same time interval of *6 h* to compare the electrical and dielectric properties of the samples. The samples of $Ni_xZn_{1-x}Fe_2O_4$, where $x = 1, 0.8, 0.6, 0.4, 0.2$, and 0 sintered at 400 °C are refereed as A, B, C, D, E, and F and those sintered at 900 °C are A′, B′, C′, D′, E′, and F′ in the present case, respectively.

The single-phase formation of the materials was confirmed by powder X-ray diffraction (XRD) technique. X-ray diffractogram of all the samples was recorded using an X-ray diffractometer (model Bruker D8 Advance). JEOL, Analytical Scanning Electron Microscope (model JSM-6360A) was use to record microstructure of the samples surface under study. The resistivity measurements were carried out using two probe method. Keithley's multimeter (model 2000) was used to record current through the sample keeping voltage across the sample constant at room temperature and well above Curie temperature. The frequency-dependent dielectric measurements were carried out on HIOKY 3532–50 LCR meter at room temperature.

Results and discussion

Structural properties

Ni–Zn powder samples were characterized at several stages of synthesis using XRD technique. The samples characterized before drying at 100 °C show amorphous nature. The samples dried at 100 °C show small hump at the positions of (311) and (400) peaks, which is a characteristic of spinel cubic ferrite phase. In order to get spinel cubic ferrite phase the samples were sintered at 400 °C for 6 h. The XRD patterns of each Ni–Zn composition treated at 400 °C is shown in the Fig. 1. The positions of all the Bragg peaks were used to obtain the interplaner spacing and these values were used to index the peaks. The peaks were indexed by comparing the interplanar distance with the JCPDS data [11]. All the samples show formation of single-spinel cubic phase except sample 'E'. In case of $Ni_{0.2}Zn_{0.8}Fe_2O_4$ (sample E), one extra peak of α-Fe_2O_3 is observed. Formation of second phase such as α-Fe_2O_3 is a consequence of the preferential loss of one or more divalent cation during the precipitation stage [12]. Lattice constant was calculated for each composition by analyzing the XRD patterns and given in Table 1.

The variation of lattice constant 'a' as a function of Zn concentration is shown in Fig. 2(a). It can be observed that lattice parameter increases with increasing Zn substitution for all the $Ni_x\ Zn_{1-x}\ Fe_2O_4$ except at $x = 0.2$ (sample 'E') for which one peak of hematite (α-Fe_2O_3) phase is observed. The increase in lattice parameter with increasing Zn content can be explained on the basis of the ionic radii. The radius of the Zn^{2+} (0.83 Å) ion is greater than that of the Ni^{2+} (0.78 Å) [13], which follow Vegard's law [14]. Only the sample 'E' show decrease in 'a'. The decrease in 'a' for sample 'E' may be attributed to partial oxidation of Ni^{2+} to Ni^{+3} of lower ionic radius and also due to Zn loss and O_2 release from the sample leading to lattice shrinkage. Similar lattice contraction due to presence of α-Fe_2O_3 is observed in case of Mn–Ni–Zn ferrite [15].

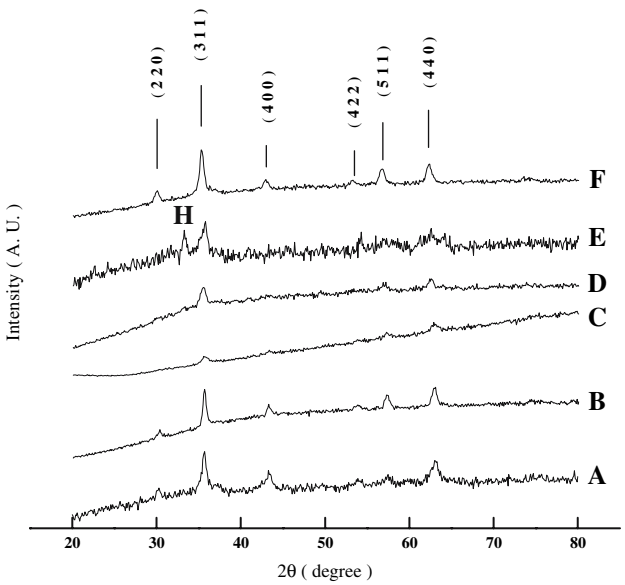

Fig. 1 (A-F) X-ray diffraction pattern of $Ni_xZn_{1-x}Fe_2O_4$ sample from $x = 1$ to $x = 0$, respectively, sintered at 400 °C. H represents hematite phase

Table 1 Lattice constant, average crystallite size, and jump length of Ni–Zn composition sintered at 400 °C

Composition	Lattice const. 'a' (Å)	Average crystalline size (nm)	Jump length L (Å)
$NiFe_2O_4$	8.3485	4.79	2.9516
$Ni_{0.8}Zn_{0.2}Fe_2O_4$	8.3658	7.69	2.9577
$Ni_{0.6}Zn_{0.4}Fe_2O_4$	8.3860	4.33	2.9649
$Ni_{0.4}Zn_{0.6}Fe_2O_4$	8.3870	4.35	2.9652
$Ni_{0.2}Zn_{0.8}Fe_2O_4$	8.3243	3.31	2.9430
$ZnFe_2O_4$	8.4480	11.7	2.9868

The crystallite size for each composition was calculated from XRD line width of (311) peak using Debye Scherrer formula, $t = 0.9\lambda/\beta\cos\theta$, where, '$t$' = crystallite size, '$\lambda$' = wavelength of X-ray, 'β'—full width at half maxima (FWHM) and 'θ' is Bragg angle. The composition-dependent crystallite size is also shown in the Fig. 2(b). The crystallite size decreases with increasing Zn concentration for the compositions 'A', 'B', 'C', 'D', and 'E', except 'F'. The increase in average crystallite size for $ZnFe_2O_4$ is due to the grain growth, indicating that the temperature required for the phase formation for Zn ferrite is less as compared to the other compositions. The crystallite size data for Ni–Zn samples sintered at 400 °C is given in Table 1.

It is known that the presence of pores may affect drastically on the physical properties of materials. In the present case experimental density was calculated using Archimedes method given by the equation

$$\text{Experimental density } (d') = [W/(W - W')] \times \text{density of the liquid} \quad (1)$$

where W—weight of the sample in air, W'—weight of the sampled in liquid. In the present case xylen was used as liquid. X-ray density (d'') was calculated using the formula

$$d'' = 8\,M/N\mathrm{a}^3 \quad (2)$$

for the spinel ferrite, where M—molecular weight of the sample, N—Avogadro's No.

$$\%\ \text{porosity} = [(d'' - d')/d''] * 100 \quad (3)$$

The composition-dependent % porosity is shown in the Fig. 2(c). It is observed that as the concentration of Zn increases the % porosity of the samples also increases. This is due to the fact that the decrease in the average particle size with increasing Zn content [16].

Figure 3(a–c) shows the scanning electron micrographs (SEM) images of $Ni_{0.8}Zn_{0.2}Fe_2O_4$ (a) as synthesized, (b) sintered at 400 °C for 6 h and (c) sintered at 900 °C for 6 h. In Fig. 3(a) it is seen that ferrite particles are of uniform size and some of the particles are agglomerated. The

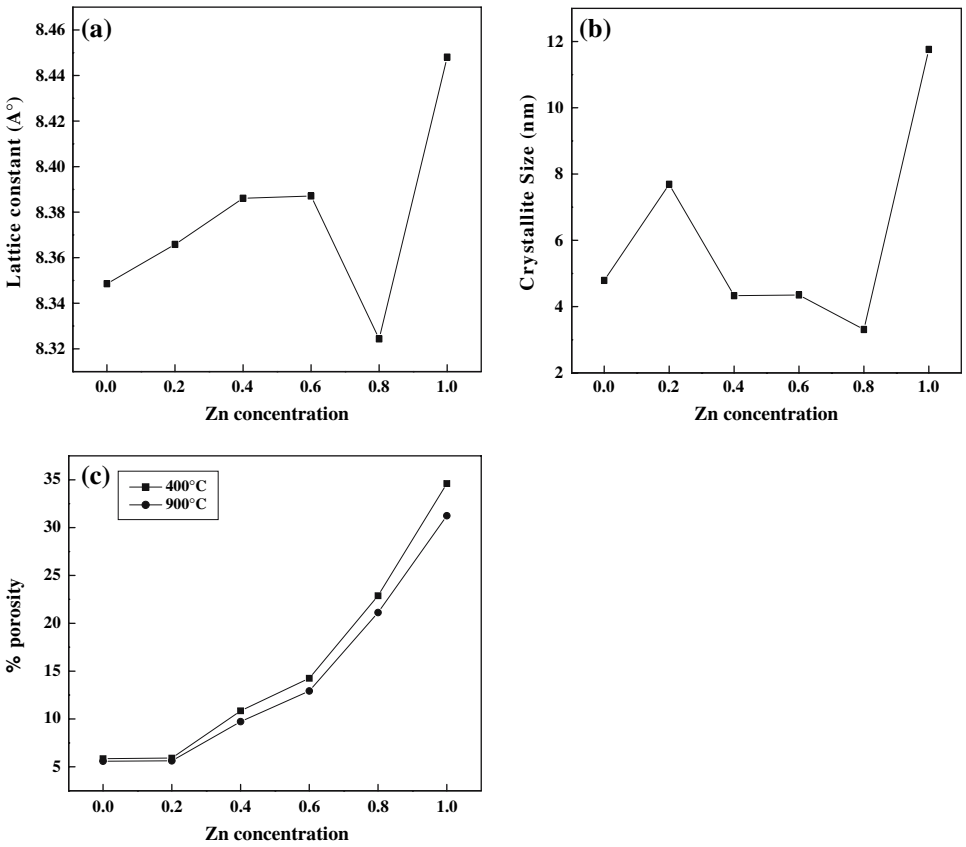

Fig. 2 (**a**) The variation of lattice constant 'a' as a function of Zn concentration. (**b**) The variation of crystalline size as a function of Zn concentration. (**c**) Composition-dependent % porosity in $Ni_xZn_{1-x}Fe_2O_4$

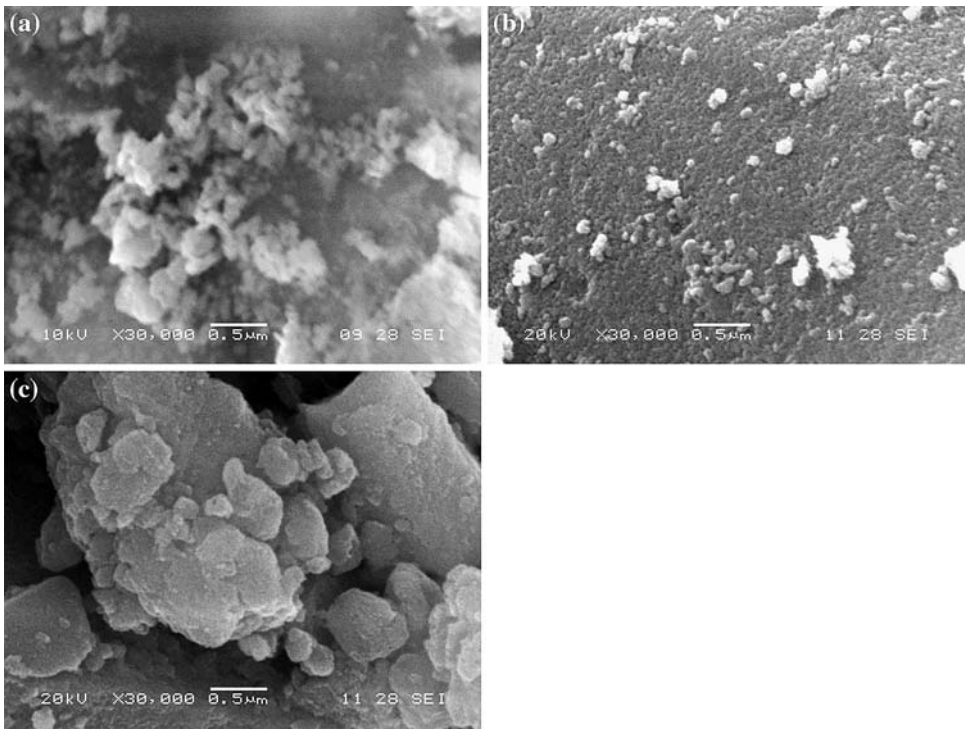

Fig. 3 (**a**) The SEM image of as synthesized $Ni_{0.8}Zn_{0.2}Fe_2O_4$. (**b**) The SEM image of $Ni_{0.8}Zn_{0.2}Fe_2O_4$ sintered at 400 °C. (**c**) The SEM image of $Ni_{0.8}Zn_{0.2}Fe_2O_4$ sintered at 900 °C

average grain size is of the order of 50 nm. The sintering temperature has a great influence on the microstructure. It is seen from Fig. 3(b, c) that, the grain size for same sample increases with increasing sintering temperature. The average grain size was 78 nm and 960 nm for the sample sintered at 400 °C and 900 °C, respectively.

Dc resistivity measurement

The composition-dependent dc resistivity of each pellet of NZFO series measured at room temperature is shown in Fig. 4. In spinel ferrite, it is known that Ni and Zn ions prefer to occupy 'B' (octahedral) and 'A' (tetrahedral) sites, respectively. Electrical resistivity is very much sensitive to cation distribution [17]. When Zn is substituted for Ni; Zn ion occupies 'A' site preferentially and equivalent iron ion migrates from 'A' site to 'B' site in place of reduced amount of Ni. This increases $Fe^{+3} \leftrightarrow Fe^{+2}$ exchange probability and thereby decrease the resistivity. Therefore, it is expected that in NZFO, substitution of Zn in place of Ni should decrease the resistivity. But, in the present case resistivity rises with increase in Zn concentration in place of Ni. The observed behavior can be explained as: In Ni–Zn spinel ferrite, conductivity is due to both 'n' and 'p' type of charge carriers. The 'n' type charge carriers are due to electron hopping between $Fe^{+3} \leftrightarrow Fe^{+2}$ and 'p' type charge carrier are due to hole hopping between $Ni^{+2} \leftrightarrow Ni^{+3}$ at octahedral site. The resistivity of the sample would be decided by the hopping of $Fe^{+3} \leftrightarrow Fe^{+2}$ and $Ni^{+2} \leftrightarrow Ni^{+3}$ probability. When Zn is substituted for Ni, it is expected to occupy tetrahedral site. However, in some cases part of Zn may occupy octahedral site [18] and part of Ni may occupy tetrahedral site. This will reduce $Fe^{+3} \leftrightarrow Fe^{+2}$ ions exchange interactions at the cost of loss of $Ni^{+2} \leftrightarrow Ni^{+3}$ exchange interactions. This result into dilution of conduction mechanism at crystallographic lattice sites in these mixed ferrites and may also contribute to the increase in dc resistivity with increase of Zn concentration [19]. Conduction mechanism in ferrite is well-explained using polaron-hopping model. Therefore, the polaron jump length is calculated for all the samples. The values of jump length 'L' calculated for various compositions are given in Table 1. This shows that 'L' increases with increasing Zn content. The observed increase in L with increase in Zn concentration supports increase in resistivity. It is seen from Fig. 4 that the Ni–Zn samples sintered at 900 °C possesses higher resistivity than that of the samples sintered at 400 °C. Normally, it is expected that resistivity of polycrystalline materials decreases with increase in grain size, i. e., resistivity should decrease with increasing sintering temperature. However, a reverse trend is observed in the present work. A similar trend was observed by Verma et al. in case of NZFO [20]. The comparatively lower values of resistivity in the samples sintered at 400 °C are possibly due to the presence of localized states in the forbidden gap, which arises due to lattice imperfections. The presence of these states effectively lowers the energy barrier to the flow of electrons. Increase in resistivity with sintering temperature can be

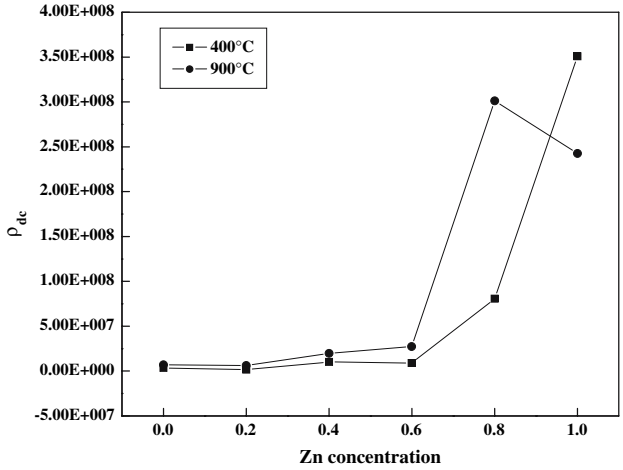

Fig. 4 Compositional dependence dc resistivity in NZFO

explained in terms of increasing structural improvement. Increased sintering temperature results in more uniform crystal structures with reduced imperfections thereby increasing sample resistivity. The effect of structural improvement is more significant than that of the anticipated effect of grain size.

The dc resistivity of polycrystalline Ni–Zn samples sintered at 400 °C and 900 °C was measured as a function of temperature from room temperature to the temperature well beyond the Curie temperature (i.e., 300–923 K). The comparison of the resistivity for the $Ni_{0.8}Zn_{0.2}Fe_2O_4$ and $Ni_{0.6}Zn_{0.4}Fe_2O_4$ samples, respectively, sintered at 400 °C and 900 °C are shown comparatively in Fig. 5(a, b), respectively. It is observed that for both the samples resistivity decreases with increasing temperature indicating the semi conducting nature of the samples. The temperature dependence of resistivity found to follow the Arrhenius equation,

$$\rho = \rho_o \exp\left(\frac{E_a}{k_T}\right) \tag{4}$$

where ρ_o is the pre-exponential factor with the dimensions of Ω cm, k is the Boltzman constant (8.617 343 × 10^{-5} eV/K), E_a is the activation energy, and T is the absolute temperature. The conduction mechanism of ferrites can be explained on the basis of the Verwey de Boer [21] mechanism that involves exchange of electrons between the ions of the same elements present in more than one valence state and distributed randomly over crystallographic lattice sites. The decrease in resistivity with increase in temperature is due to the increase in drift mobility of the charge carriers. Also conduction in ferrites is attributed to hopping of electrons from $Fe^{3+}$to Fe^{2+} at elevated temperatures [22].

It can be seen that for both the samples variation of resistivity with increasing temperature follow the same trend. For spinel ferrite samples usually three linear regions are observed in the ln ρ vs. 1/T plot from room temperature to well above Curie temperature [23–25]. The change in slope indicates change in conduction mechanism. The first low-temperature region (up to about 423 K) is attribute to the conduction due to impurities, voids, defects, etc. The second temperature region (up to Curie temperature) is attributed to ferrimagnetic region. Third temperature region (above Curie temperature) is attributed to paramagnetic region [23–25]. In the present case first region agrees with the reports in the literature. In the temperature range 600–800 K the plot deviated from linearity, which is unusual. The temperature region above 800 K again follows linearity.

The activation energies for conduction are computed from $\log_{10} \rho_{dc}$ verses 1000/T plots for all the samples, and the data is given in Table 2. In Table 2 it is seen that the activation energy decreases at higher sintering temperature. Higher values of activation energy have been found to correspond to low conductivity values of samples, with increasing Zn concentration.

It is important to note that small changes in ΔE with x are observed for the present system. According to Ahmed et al. [26], the effect of x on ΔE is greater if the substituted

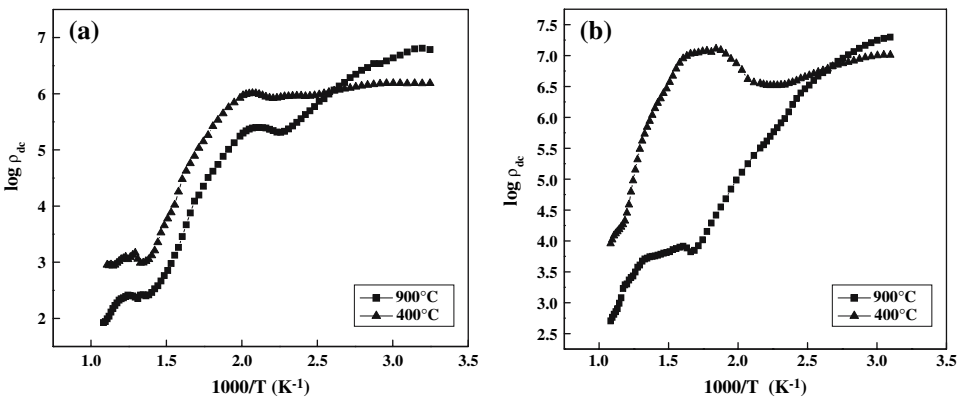

Fig. 5 (**a**) Comparison of variation of log dc resistivity of $Ni_{0.8}Zn_{0.2}Fe_2O_4$ with temperature inverse; sintered at 400 ° C and at 900 ° C. (**b**) Comparison of variation of log dc resistivity of $Ni_{0.6}Zn_{0.4}Fe_2O_4$ with temperature inverse; sintered at 400 °C and at 900 °C

Table 2 Resistivity, activation energy, and % porosity comparison of Ni_x $Zn_{(1-x)}$ Fe_2O_4 sample sintered at 400 °C and 900 °C

Composition	ρ_{dc} MΩ cm 400 °C	ρ_{dc} MΩ cm 900 °C	Activation energy ΔE (eV) 400 °C	Activation energy ΔE (eV) 900 °C	% porosity (gm/cm^3) 400 °C	% porosity (gm/cm^3) 900 °C
$NiFe_2O_4$	3.4921	6.9884	0.3331	0.1724	5.858	5.582
$Ni_{0.8}Zn_{0.2}Fe_2O_4$	1.5212	6.1286	0.1847	0.2677	5.908	5.621
$Ni_{0.6}Zn_{0.4}Fe_2O_4$	10.2233	19.8405	0.2851	0.1392	10.847	9.724
$Ni_{0.4}Zn_{0.6}Fe_2O_4$	8.8368	27.3442	0.2273	0.1615	14.248	12.925
$Ni_{0.2}Zn_{0.8}Fe_2O_4$	8.0689	30.1190	0.2140	0.2026	22.884	21.124
$ZnFe_2O_4$	35.9534	24.2480	0.4230	0.1803	34.601	31.245

cation occupy B-sites. Devale et al. [27] suggest that almost no change in E is observed when the substitution is made on A-sites without disturbing the B-sites. Therefore, the present results suggest that substitution of Zn in place of Ni affects cation distribution at octahedral site. The unusual behavior observed in the temperature range 600–800 K can be explained as: It is expected that in NZFO both Ni^{+2} and Zn^{+2} ions occupy to octahedral site and tetrahedral site respectively, and Fe^{+3} ions are expected to occupy tetrahedral and octahedral site. Our room temperature resistivity data suggest that Zn^{+2} ion may occupy octahedral site. Kim et al., based on mossbaure spectra analysis reported that for Ni–Co spinel ferrite system an alteration of occupancy of Ni, Co ions to tetrahedral site instead of octahedral site [28]. Altering the cation distribution between the chemically inequivalent sites will not lead to change crystal structure and chemical composition, but will affect the electrical properties. The present study therefore indicates that a ferrite with a particular composition may have different cation distribution in its bulk phase than that in its nanoparticle phase. When temperature is increased above 500 K slowly migration of Fe^{+3}, Ni^{+2} ions from A site to the B site starts at the cost of migration of Zn^{+2} from octahedral site to tetrahedral site. Migration of Fe^{+3}, Ni^{+2} ions to octahedral site increase $Fe^{+3} \leftrightarrow Fe^{+2}$ and $Ni^{+2} \leftrightarrow Ni^{+3}$hopping probability, which results in decreased resistivity values. The migration processes increases up to 700 K and afterwards it saturates [28]. This results an anomaly in the resistivity behavior in the temperature region 600–800 K. Similar results were obtained for Ni–Co ferrite synthesized by chemical co-precipitation technique by us [29].

Dielectric properties

Figure 6(a, b) shows variation of ε‘ with frequency for the $Ni_{1-x}Zn_xFe_2O_4$ samples sintered at 400 °C and 900 °C, respectively. Initially ε‘ decreases with increase in frequency and finally at higher frequencies reaching a constant value for all the compositions. This is obvious because of the fact that the species contributing to the polarizability are lagging behind the applied field at higher frequency. The variation of ε‘ with frequency reveals the dispersion due to Maxwell–Wagner [30, 31] type interfacial polarization, which is in agreement with Koop's phenomenological theory [32]. According to these models, the dielectric material with a heterogeneous structure can be imagined as a structure consists of well-conducting grains separated by highly resistive thin layers (grain boundaries). In this case, the applied voltage on the sample drops mainly across the grain boundaries and a space charge polarization is built up at the grain boundaries. The space charge polarization is governed by the available free charges on the grain boundary and the conductivity of the sample. Koop proposed that the effect of grain boundaries is predominant at lower frequencies. The thinner the grain boundary, the higher the dielectric constant value is. The observed decrease of ε‘ with increasing the frequency can be attributed to the fact that the electron exchange between Fe^{+2} and Fe^{+3} ions cannot follow the change of the external applied filed beyond a certain frequency [33]. According to Novikava et al. [34] the polarization in ferrite is thought a mechanism similar to conduction process.

Figure 6(c, d) shows variation of tan δ with frequency for the $Ni_{1-x}Zn_xFe_2O_4$ samples; sintered at 400 °C and 900 °C, respectively. It is seen from the Fig. 6(c, d) that tan δ decreases with increasing frequency with shoulder nature for A, C, D, and A'. The observation of shoulder indicates the presence of resonance between the hopping frequency of the charge carriers and applied frequency. For other samples, shoulder behavior is not observed in the measured frequency range. This may be due to the resonance frequency for other samples lie beyond the frequency range of measurements. The value of tan δ is less for the samples sintered at 900 °C as compared to that of the samples sintered at 400 °C. The dispersion behavior observed can be explained on similar line to that of ε‘ variation with frequency.

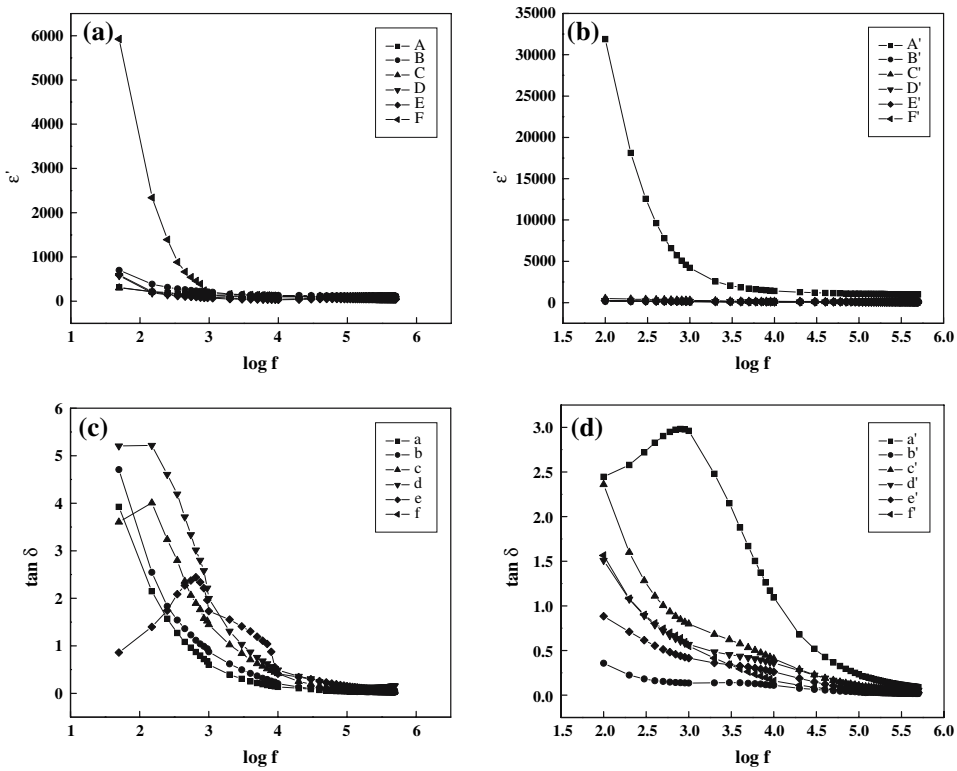

Fig. 6 (**a**) Variation of ε' with frequency at room temperature for $Ni_xZn_{1-x}Fe_2O_4$ sintered at 400 °C. (**b**) Variation of ε' with frequency at room temperature for $Ni_xZn_{1-x}Fe_2O_4$ sintered at 900 °C. (**c**) Variation of loss tangent with frequency at room temperature for $Ni_xZn_{1-x}Fe_2O_4$ sintered at 400 °C. (**d**) Variation of loss tangent with frequency at room temperature for $Ni_xZn_{1-x}Fe_2O_4$ sintered at 900 °C

Conclusions

Samples of nanocrystalline $Ni_xZn_{1-x}Fe_2O_4$ have been successfully synthesized using chemical co-precipitation method and effect of sintering temperature on the morphological, electrical, and dielectrical properties have been studied. It is observed from XRD analysis that ferrite phase is formed at as low temperature as 400 °C without formation of unidentified phase. The microstructure study from SEM shows that the grain size increases with sintering temperature. % porosity and resistivity of the samples were dependent on Zn concentration. The nature of dc resistivity with temperature at different sintering temperatures clearly shows the change in conduction behavior of the same sample. The anomalous behavior is due to change in cation distribution. Study of dielectric properties with frequency at room temperature helps in understanding the electric behavior of the samples.

Acknowledgements A.D. Sheikh is thankful to DST, New Delhi, for the award of JRF fellowship. V.L. Mathe is thankful to DST, New Delhi, for the financial support, FAST TRACK young scientist fellowship, and BOYSCAST fellowship.

References

1. Slick PI (1980) In: Wohlfrath EP (ed) Ferromagnetic materials, vol 2. North hollond, Amsterdam, p 196 and references there in
2. Ferrites: Proceedings of sixth international conference on ferrites (ICF6), Yamaguchi T, Abe M (eds) The Japan society of powder and powder Metallurgy, Japan, 1992
3. Morrison SA, Cahill CL, Carpenter EE, Calvin S, Swaminathan R, McHenry ME, Harris VG (2004) J Appl Phys 95:6392
4. Daniels JM, Rosencwaig A (1970) Can J Phys 48:381
5. Stoppels D (1996) J Magn Magn Mater 160:323
6. Lee KH, Cho DH, Jeung SS (1997) J Mater Sci Lett 16:83
7. Kim CS, Yi YS, Park K-T, Namgung H, Lee JG (1999) J Appl Phys 85:5223
8. Srivastava AK, Hurben MJ, Wittenauer MA, Kabos P, Patton CE, Rameh R, Dorsey PC, Chrisey DB (1999) J Appl Phys 85:7838
9. Amado MM, Rogalsk MS, Guimaraes L, Sousa JB, Bibicu I, Welch RG, Palmer SB (1998) J Appl Phys 83:6852
10. Sheikh AD, Kamble RB, Mathe VL (2006) Proc DAE solid state phys symp 51:235
11. JCPDS card no of $NiFe_2O_4$ 10-325
12. Rath C, Sahu KK, Anand S, Date SK, Mishra NC, Das RP (1999) J Magn Magn Mater 202:77
13. Raghavan V (2004) Materials Science and Engineering, 5th edn. Prentice–Hall of India, New Delhi
14. Komar AP (1954) Bull Acad Sci USSR Ser Phys 18:122
15. Verma A, Chatterjee R (2006) J Magn Magn Mater 306:313
16. Mahmud ST, Akther Hossain AKM, Abudul Hakim AKM, Seki M, Kawai T, Tabata H (2006) J Magn Magn Mater 305:269
17. Puri RK, Sayen V (1989) Proceedings ICF-5, India 245
18. Jeyadevan B, Tohji K, Nakatsuka K (1994) J Appl Phys 76:6325
19. Varshney U, Churachill RT, Puri RK, Mendiratta RG (1989) Proceedings ICF-5, India 255
20. Verma A, Goel TC, Mendiratta RG, Gupta RG (1999) J Magn Magn Mater 192:271
21. Verwey EJ, de Boer JH (1936) Rec Trans Chim Phys Bas 55:531
22. Vishwanathan B, Murthy VRK (1990) Ferrite materials: science and technology. Narosa Publication House, New Delhi
23. Liu Y-L, Liu Z-M, Yang Y, Yang H-F, Shen G-L, Yu R-Q (2005) Sens Actuators B 107:600

24. Solyman S (2006) Ceram Int 32:755
25. Patil MG, Mahajan VC, Ghatage AK, Patil SA (1996) Ind J Pure Appl Phys 34:1665
26. Ahmed MA, Nimr MK, Tawfik A, Hasab AM (1991) Phys Status Solid A 123:501
27. Devale AB (1980) Ph. D. Thesis IISc, Nagpur Uni. India
28. Kim CS, Lee SW, Park SL (1996) J Appl Phys 79:5428
29. Mathe VL, Kamble RB (2007) Mater Res Bull In Press
30. Maxwell JC (1973) Electricity and magnesium, vol 1. Oxford University press, New york, p 828
31. Wagner KW (1973) Am Phys 40:817
32. Koop CG (1951) Phys Rev 85:121
33. Zemansky MW (1968) Heat and thermodynamics. McGraw Hill, New York, p 460
34. Rabinikin LT, Novikova ZI (1960) Ferrites, Acad. Naok. USSR, Minsk 146